# Formation of nanoporous platinum by selective dissolution of Cu from $Cu_{0.75}Pt_{0.25}$

D.V. Pugh, A. Dursun, and S.G. Corcoran
*Virginia Polytechnic Institute & State University, Department of Materials Science and Engineering, Blacksburg, Virginia 24061-0286*

(Received 17 September 2002; accepted 30 October 2002)

This paper gives results demonstrating the production of nanoporous platinum through the de-alloying of $Cu_{0.75}Pt_{0.25}$ alloy in 1 M $H_2SO_4$. Both field emission scanning electron microscopy and small angle neutron scattering confirm the presence of porosity with a diameter of approximately 3.4 nm. This is the smallest porosity quantitatively reported from a de-alloying process to date. The small size is attributed to the extremely small values of surface diffusivity expected for Pt at room temperature, effectively eliminating room-temperature coarsening processes. The results also show that larger length scales can be achieved through coarsening at elevated temperatures. The ease of production of porous platinum makes it attractive for possible applications, such as high surface area electrodes for biomedical devices or as catalyst materials.

## I. INTRODUCTION

Selective dissolution of one or more elements from an alloy is achieved through a corrosion process known as de-alloying. Consider a binary alloy, $A_pB_{1-p}$, where the reactivities of A and B are significantly different relative to a specific corrosive environment, and element A is more reactive. Under the appropriate driving force (applied voltage or presence of oxidizing species), we can selectively remove A from the alloy. The alloy will now evolve in one of two directions. At moderate driving force, the alloy surface will enrich in component B, resulting in a protective B-rich layer and thus hindering further dissolution. However, at a slightly higher driving force, a structural instability occurs, resulting in the formation of porosity. This porosity allows for the ingress of the corrosive environment and a continuation of the process. We are unaware of any investigations that define the limit of the depth of porosity that can be created, but it has been demonstrated that depths of 2 mm are easily achievable.[1] The mechanism of the structural instability that leads to porosity formation has been the focus of many recent investigations.[2,3]

De-alloying has been observed in numerous systems including Cu–Au,[4–8] Zn–Cu,[4,9–11] Mg–Cd,[12,13] Al–Cu,[9] Ag–Au,[1,14–21] Mn–Cu,[9,22] Pd–Cu,[23] Ni–Cu,[9] and even during the reduction of titanium dioxide in molten calcium chloride.[24,25] Beyond its potential for the creation of new porous materials, a better understanding of the de-alloying processes is relevant to stress corrosion cracking of some alloy, alloy-environment systems (see for example Refs. 26–31), the accelerated corrosion in AA2024-T3,[32,33] corrosion of austenitic stainless steel in acidified chloride containing electrolyte,[27,34] and the production of Raney metal catalysts.[35,36]

The morphology of typical de-alloyed structures consists of a highly tortuous, completely interconnected porosity with a pore diameter as small as 3 nm. The structure can be coarsened to larger length scales (up to micrometers) at elevated temperatures[1] and has been shown to coarsen at room temperature (to size scales as large as a few 100 nm in the case of Au)[16,18–21,37] as a function of the applied voltage[16,20] and electrolyte composition.[15]

From an applications viewpoint, the question remains, "How universal is this behavior?" That is, can we design new porous materials based on our current understanding of the de-alloying process in such model systems as Ag–Au? This paper shows a step in this direction by demonstrating the ability to produce nanoporous Pt through the selective dissolution of Cu from a $Cu_{0.75}$–$Pt_{0.25}$ alloy. The interest in developing nanoporous Pt is motivated by our interest in developing alternative processing routes for the creation of high surface area electrodes for biomedical applications.

In general, de-alloying in Pt-based systems has been virtually unexplored. Simmonds *et al.*[38] observed selective removal of Al from sputter-deposited Pt–Al thin films immersed in 4 M NaOH at 300 K as evidenced through compositional analysis, indicating an enrichment of Pt after exposure to NaOH. The presence of porosity was not confirmed. The Pt–Al system was not chosen in our investigation because the presence of multiple

 

intermetallic phases complicates fundamental studies on the de-alloying process. Pickering *et al.*[39] investigated the de-alloying of $Pt_{0.1}Co_{0.9}$ exposed to HCl gas at elevated temperatures (900–1300 K) and confirmed the presence of porosity. Due to the elevated temperatures required for the de-alloying in this system, only microporous platinum was demonstrated.

## II. EXPERIMENTAL

The alloy samples were prepared at Ames Laboratory (Ames, IA) by arc melting the Cu (99.999% pure) and Pt (99.99% pure) on a water-cooled copper hearth plate in a reduced pressure atmosphere of argon. The alloy was then heat treated and drop quenched into an oil bath at 1000 °C to avoid the formation of ordered phases. After quenching, the alloy was cold rolled to a thickness of 200 μm. The rolled foil was then annealed at 1000 °C for 1.5 h and quenched by removing it from the inert atmosphere furnace and allowing it to cool in a stream of blowing air.

Prior to use in the electrochemical cell, the foils were cut into 2 × 3 cm samples and masked with Teflon tape to a known exposed area. The electrolyte consisted of reagent-grade 1 M sulfuric acid; two platinum counter electrodes parallel to the alloy's exposed area were used along with a saturated calomel electrode (SCE) as a reference. A Luggin probe was used to avoid contamination of chlorides into the solution. A model 263A Potentiostat from Princeton Applied Research (Oakridge, TN) was used for all experiments. Typically, the potential was scanned at a rate of 1 mV/s from open circuit to the desired de-alloying potential. The samples were then rinsed in deionized water prepared with a Barnstead Nanopure system with a specific resistivity of 18.2 MΩ cm.

Small angle neutron scattering (SANS) experiments were conducted at the National Institute of Standards and Technology 20 MW reactor in Gaithersburg, MD. The samples were placed in an evacuated chamber in transmission geometry. The measurements were performed using a 30-m-long SANS instrument (typically NG7). The wavelength of the incident neutrons was 6 Å. The measurement range for the scattering vector $Q$ was (0.009–0.174) $Å^{-1}$ where

$$|Q| = \frac{4\pi}{\lambda_{\text{neutrons}}} \sin\Theta \quad .$$

Field emission scanning electron microscopy (FESEM) was performed with a LEO 1550.

## III. RESULTS AND DISCUSSION

### A. Alloy selection considerations

Based on our experience with the system Ag–Au and the literature for other de-alloying systems, we believe we can identify two general requirements for alloy systems to undergo porosity formation during selective dissolution. First, the alloy $A_pB_{1-p}$ should exist as a single-phase solid solution at a value of $p$ of at least 20 at.% but more typically in range of 60–80 at.%. The minimum value of $p$ is dependent upon the relative rates of dissolution of A and surface diffusivity of B[2]; e.g., for Zn–Cu where there is relatively large difference in the metal/metal-ion equilibrium potentials the value $p$ is approximately 18 at.%,[40] while for Ag–Au where the equilibrium potential for Ag is relatively close to the oxidation potential for Au, the value $p$ is much higher at approximately 60 at.%.[41] If multiple phases exist in the alloy, porosity formation of any individual phase would follow the same requirement, and hence typically only the A-rich phase would de-alloy. In this case, de-alloying would be isolated to only surface grains unless a mechanism existed for the penetration of the electrolyte throughout the alloy; for example, the A-rich grains form a percolating path through the alloy. The de-alloying in multiple phase alloys from this perspective has not been investigated to date. The second condition for porosity formation is that an electrochemical environment can be found in which the dissolution rate of A is significantly greater than the dissolution rate of B (ideally B undergoes no dissolution). One easy scenario to accomplish this condition is to select two elements that have significantly different corrosion potentials and then drive the alloy system with a corrosion potential significantly greater than the potential of A but less than that for B. This is the approach taken in this paper.

Considering the above criteria, we chose $Cu_{0.75}Pt_{0.25}$ as our model system. The Pt–Cu system exists as a single-phase solid solution for all compositions, and the dissolution of Cu is easily driven in acid electrolytes at potentials where Pt is highly stable.

### B. Electrochemical results

The electrochemical behavior of $Cu_{0.75}Pt_{0.25}$ in 1 M $H_2SO_4$ is shown in Fig. 1. The inset in Fig. 1 shows the same data on a linear scale over a narrow range of potential. The value of the current density gives the total electrochemical reaction rate occurring at a given potential. For values of potential in the range of 0.4–1.0 V, secondary electrochemical reactions on Pt occur with values less than 1–2 μA $cm^{-2}$. From 1.0 V to approximately 1.2 V the onset of Pt oxidation and oxygen evolution increases the current density to approximately 10 μA $cm^{-2}$, which is still significantly lower than the de-alloying currents observed in Fig. 1. If we then make the approximation that the anodic current is due solely to the Cu dissolution reaction, we can convert the current density into a Cu dissolution rate through Faraday's law. Under this assumption, a current density of 100 μA $cm^{-2}$

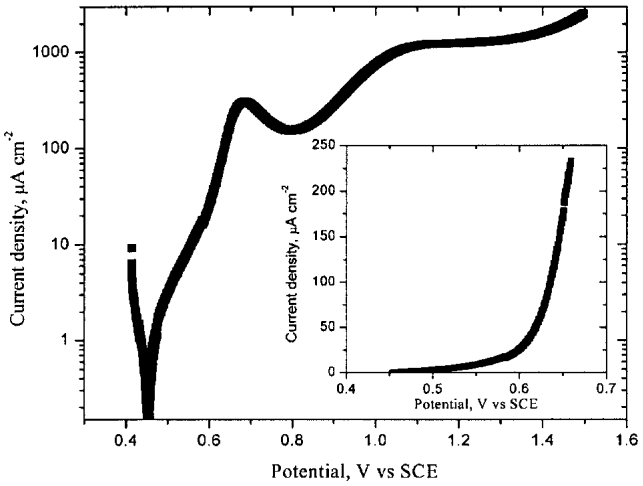


FIG. 1. Alloy polarization curve for 75/25 CuPt alloy in dearated 1M $H_2SO_4$, scan rate 1 mV/s. Inset shows current density on a linear scale near the critical potential.

corresponds to a Cu dissolution rate of $3 \times 10^{14}$ atoms $cm^{-2}$ $sec^{-1}$ or a porosity formation rate of approximately 180 nm $h^{-1}$.

The rapid increase in the dissolution rate observed in the inset of Fig. 1 at a potential of approximately 0.6 V SCE is indicative of the onset of de-alloying and is referred to in the literature as the de-alloying critical potential.[29] If we hold the potential of the alloy below this value, the current will rapidly decay as the surface enriches in Pt; within several minutes the current density approaches μA $cm^{-2}$ values. Above this potential, the de-alloying current increases with time during a potential hold and maintains de-alloying currents in the mA $cm^{-2}$ range. All samples held above the critical potential result in the formation of porosity as confirmed by FESEM and SANS. These results are discussed below.

### C. Morphological characterization

Figure 2(a) is a FESEM image of nanoporous platinum created by the de-alloying of $Cu_{0.75}Pt_{0.25}$ at 1.2 V SCE in 1 M $H_2SO_4$ for 2.4 h. The quality of the image is poor since we are at the limit of resolution of the FESEM, but the presence of porosity is evident. From the image, we can estimate the pore diameter to be 3.5–4.0 nm. To provide confirmation of the bicontinuous nature of the porosity, a dealloyed sample identical to that shown in Fig. 2(a) was heat treated for 60 min at 500 °C. The heat treatment coarsened the porosity to length scales easily observable in the FESEM, as shown in Fig. 2(b). The 60 min heat treatment resulted in porosity on the order of 100 nm in diameter. Porosity of varying length scales can be created through similar heat treatment procedures as a function of time and temperature.[42] Porosity on the scale of many microns has been demonstrated

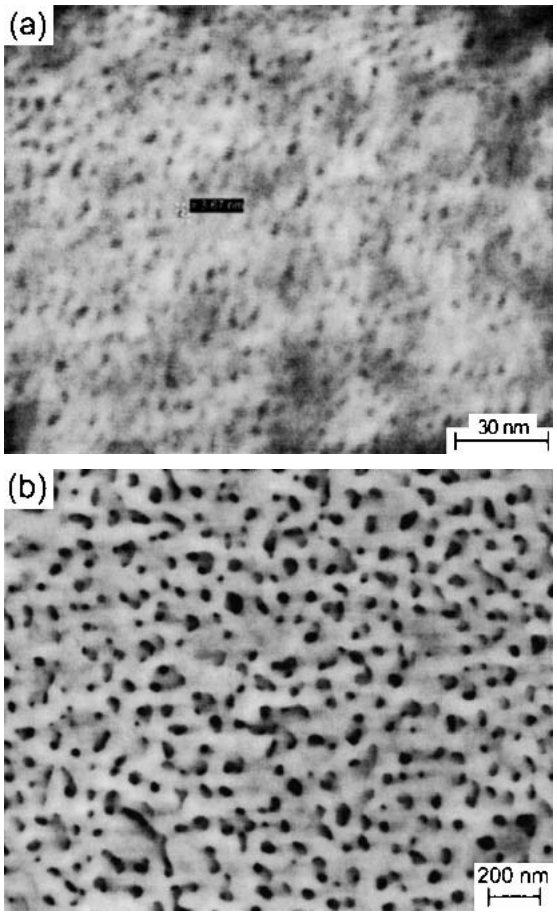


FIG. 2. Porous Pt created by selectively dissolving Cu from $Cu_{0.75}Pt_{0.25}$ at 1.2 V SCE in 1 M $H_2SO_4$ for 2.4 h (a) as de-alloyed and (b) coarsened at 500 °C for 60 min.

in our laboratory and by others for dealloyed Au structures.[1] To better quantify the room temperature porosity, we performed neutron scattering measurements at the National Institute of Standards and Technology Center for Neutron Research in Gaithersburg, MD, as discussed below.

Previously we demonstrated that SANS is ideal for characterizing the morphology of nanoporous metals[19–21] in the 1–200 nm range, and with the more recent development of ultra-small angle neutron scattering (USANS) porosity as large as 10 μm can be characterized.[43] A detailed discussion of the use of SANS for the characterization of de-alloying in both *in-situ* and *ex-situ* investigations is in progress.[44] The method is briefly reviewed here. SANS from nanoporous metals closely resembles that of the scattering from microemulsions[45] and spinodally decomposed materials,[46] all of which display a bicontinuous morphology. In the case of microemulsions, we have continuous water and oil phases, while for de-alloyed structures we have continuous phases of metal and void. Interestingly, the scattering from such structures results in a peak in the

scattering intensity data. Figure 3 demonstrates this for the scattering from porous Pt produced by de-alloying $Cu_{0.75}Pt_{0.25}$ at 1.2 V SCE in 1 M $H_2SO_4$ for 2.4 h. The inset shows the same data on a linear scale. The fit to the data, which will be discussed below, is shown by the solid line. The presence of a peak indicates that the morphology contains a well-defined average length scale and was first explained by Berk *et al.*[47] If we take a simple approach and associate this length scale as being the sum of the pore and ligament length, we can approximate this length as $2\pi/Q_p$ where $Q_p$ is the position of the peak in Fig. 3. This gives a value of 7 nm. If we take the pore size to be approximately half of this value, we expect porosity on the order of 3.5 nm. We now discuss a more rigorous analysis of the scattering data.

The scattering from bicontinuous morphologies was treated by Berk[46,47] and Chen.[48,49] In this paper, we follow the analysis of Berk *et al.* since it allows for the generation of real space images. In the Berk analysis, the bicontinuous morphology is mathematically modeled as a three-dimensional continuous contour of a stochastic standing wave following the development by Cahn[50] for describing the morphology of spinodally decomposed systems. This standing wave $S_N(\boldsymbol{r})$ is generated by summing a large number $N$ of plane waves with random amplitudes $A$, wavevector directions $\hat{k}_n$, and phase constants $\phi_n$, and is given by:

$$S_N(\boldsymbol{r}) = \frac{1}{(N\langle A^2\rangle)^{1/2}} \sum_{n=1}^{N} A_n \cos\left(\frac{2\pi}{\lambda}\,\hat{k}_n \times \boldsymbol{r} + \phi_n\right) \quad .$$

The only adjustable value in this equation is the wavelength $\lambda$. Note this $\lambda$ is the well-defined length scale intrinsic to the morphology that results in the scattering peak. For a single value of $\lambda$, the scattering results in a Bragg-like peak at a $Q$ value of $2\pi/\lambda$, although the real space structure still consists of a random bicontinuous morphology. By adding dispersion into the values chosen for $\lambda$, the scattering peak broadens and resembles that measured experimentally. The normalization in $S_N(\boldsymbol{r})$ is chosen such that $0 \leqslant S_N(\mathbf{r}) \leqslant 1$. If we now choose a value $\alpha$, such that $0 \leqslant \alpha \leqslant 1$ and assign all positions $\mathbf{r}$ in real space, which have a value of $S_N(\boldsymbol{r}) > \alpha$ as metal and all positions with a value of $S_N(\boldsymbol{r}) < \alpha$ as void, we generate a real space three-dimensional bicontinuous structure, as shown in Fig. 4. The scattering from such a structure can then be calculated and compared to the experimental data. The value for $\lambda$ and dispersion is adjusted until a good fit is found. The result is a fit to the data and a real space representation of the structure that can then be analyzed directly for determining pore-size distribution, metal ligament size distribution, and surface area.

The fit using this model to our data is shown by the solid line in Fig. 3. This fit had $\alpha = 0.477$ corresponding to a pore fraction of 75% and a $k_{mean} = 2\pi/\lambda = 0.11617$ Å$^{-1}$, and the dispersion about this mean followed a log normal distribution with a $\sigma = 0.360$. The three-dimensional real space structure corresponding to this fit is shown in Fig. 4. A two-dimensional slice through the corresponding real space structure is shown in Fig. 5. An average pore size of 3.4 nm was obtained from this figure by making chord length measurements on the image. This represents the smallest ligament sizes that we obtained in a de-alloyed structure. Under approximately the same set of conditions, Ag-Au alloys display pore sizes in the range of 8–20 nm depending upon the de-alloying potential;[14] this increase in pore size is due mainly to the greater values of surface diffusivity expected for Au as compared to Pt.

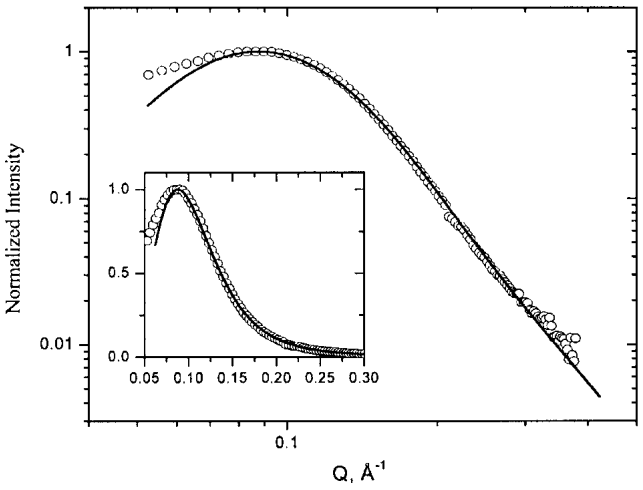


FIG. 3. SANS data for dealloyed Pt (circles) and fit (solid line) to data using the Berk model. Inset shows the data and fit on linear.

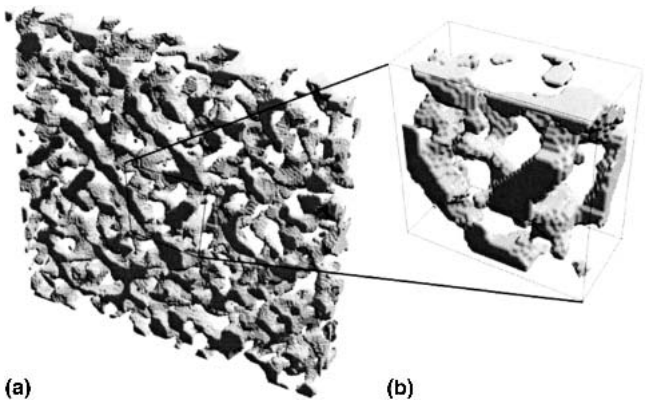


FIG. 4. Simulation of porous Pt calculated from the fit to the SANS data of Fig. 3. (a) Three-dimensional slice of size 56 × 56 × 7 nm and (b) magnified view of the structure 14 × 14 × 7 nm. Note that the pixel spacing used in the calculation of this image, which results in the fine scale structure observed, was chosen as 0.28 nm (the atomic radius of a Pt atom).

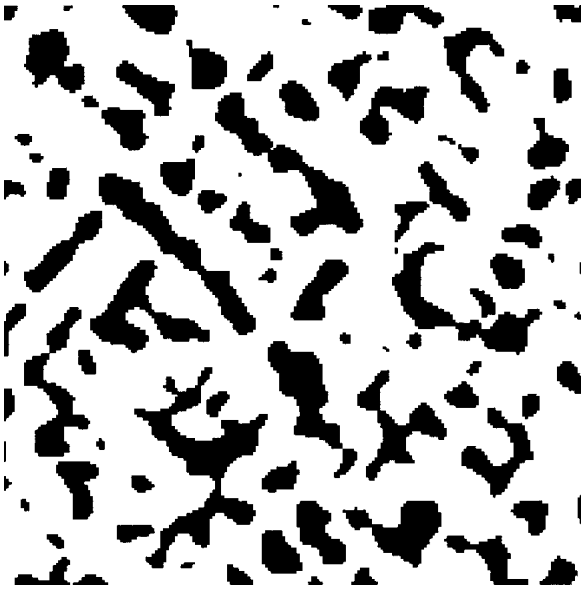

FIG. 5. Two-dimensional slice with a thickness of 0.28 nm through the simulation of Fig. 4. This image was used in the calculation of pore and metal ligament sizes through chord distribution measurements.

## IV. CONCLUSIONS

The production of nanoporous platinum through the selective dissolution at room temperature of Cu from $Cu_{0.75}Pt_{0.25}$ was demonstrated. Both FESEM and SANS analysis confirmed the presence of porosity with a diameter of approximately 3.4 nm. This is the smallest porosity reported from a de-alloying process to date. The small size was attributed to the extremely small values of surface diffusivity expected for Pt at room temperature, effectively eliminating room-temperature coarsening processes. It was also shown that larger length scales can be achieved through coarsening at elevated temperatures. The ease of production of porous platinum may make this method of processing attractive for applications such as high surface area biomedical electrodes or as catalyst materials.

## ACKNOWLEDGMENTS

The authors would like to acknowledge funding from the National Science Foundation (NSF) under Contract No. DMR-9975190. The authors also thank John Barker of the National Institute of Standards and Technology (NIST) Center for Neutron Scattering Research for his invaluable assistance on the operation of the neutron beam-line and many discussions on SANS analysis. We acknowledge the support of NIST, the United States Department of Commerce, in providing facilities used in this work. This material is based upon activities supported by the NSF under Agreement No. DMR-9986442.

## REFERENCES

1. R. Li and K. Sieradzki, Phys. Rev. Lett. **68,** 1168 (1992).
2. K. Sieradzki, N. Dimitrov, D. Movrin, C. McCall, N. Vasiljevic, and J. Erlebacher, J. Electrochem. Soc. **149,** 370 (2002).
3. J. Erlebacher, M.J. Aziz, A. Karma, N. Dimitrov, and K. Sieradzki, Nature **410,** 450 (2001).
4. H. W. Pickering, in *Fundamental Aspects of Stress Corrosion Cracking*, edited by R.W. Staehle, A.J. Forty, and D. van Rooyen (NACE International, Ohio State University, 1967), pp. 159–177.
5. T.P. Moffat, F-R.F. Fan, and A.J. Bard, J. Electrochem. Soc. **138,** 3224 (1991).
6. J.D. Fritz and H.W. Pickering, J. Electrochem. Soc. **138,** 3209 (1991).
7. B.G. Ateya, J.D. Fritz, and H.W. Pickering, J. Electrochem. Soc. **144,** 2606 (1997).
8. P.R. Swann, Corrosion **25,** 147 (1969).
9. M.J. Pryor and J.C. Fister, J. Electrochem. Soc. **131,** 1230 (1984).
10. H.W. Pickering and C. Wagner, J. Electrochem. Soc. **114,** 698 (1967).
11. R.B. Abrams, Trans. Am. Chem. Soc. **42,** 39 (1922).
12. J.I. Gardiazabal and J.R. Galvele, J. Electrochem. Soc. **127,** 255 (1980).
13. J.I. Gardiazabal and J.R. Galvele, J. Electrochem. Soc. **127,** 259 (1980).
14. A. Dursun, D.V. Pugh, and S.G. Corcoran, (unpublished).
15. A.J. Forty and P. Durkin, Philos. Mag. A **42,** 295 (1980).
16. R.G. Kelly, A.J. Young, and R.C. Newman, in *Electrochemical Impedance: Analysis and Interpretation,* edited by J.R. Scully, D.C. Silverman and M.W. Kendig (ASTM STP **1188,** American Society for Testing and Materials, Philadelphia, PA 1993), pp. 94–112.
17. K. Sieradzki, J. Electrochem. Soc. **140,** 2868 (1993).
18. K. Sieradzki, R.R. Corderman, K. Shukla, and R.C. Newman, Philos. Mag. A **59,** 713 (1989).
19. S.G. Corcoran, K. Sieradzki, and D. Wiesler, in *Proceedings of the Symposium on Scattering for Materials Science II*, edited by D.A. Neumann, T.P. Russell, and B.J. Wuensch (Materials Research Society, Pittsburgh, PA, 1994), pp. 377–382.a
20. S.G. Corcoran, D.G. Wiesler, and K. Sieradzki, in *Electrochemical Synthesis and Modification of Materials,* edited by P.C. Andricacos, S.G. Concoran, J-L. Delplanete, T.P. Moffat, and P.C. Searson (Mater. Res. Soc. Symp. Proc. **451**, Pittsburgh, PA, 1997), pp. 93–98.
21. S.G. Corcoran, in *Proceedings of the Symposium on Critical Factors in Localized Corrosion III*, edited by R.G. Kelly, G.S. Frankel, P.M. Natishan, and R.C. Newman (The Electrochemical Society, Pennington, NJ, 1999), pp. 500–507.
22. K. Sieradzki and R. Li (unpublished).
23. B. Kabius, H. Kaiser, and H. Kaesche, in *Surfaces, Inhibition, and Passivation: Proceedings of an International Symposium Honoring Doctor Norman Hackerman on His Seventy-fifth Birthday,* edited by E. McCafferty and R.J. Brodd (Electrochemical Society, Penington, NJ, 1986), pp. 562–573.
24. G.Z. Chen, D.J. Fray, and T.W. Farthing, Nature **407**, 361 (2000).
25. D.J. Fray, MRS Bull. **25**(12), 11 (2000).
26. K. Sieradzki and R.C. Newman, Philos. Mag. A **51,** 95 (1985).
27. R.C. Newman, R.R. Corderman, and K. Sieradzki, Brit. Corrosion J. **24,** 143 (1989).
28. D.E. Williams, R.C. Newman, Q. Song, and R.G. Kelly, Nature **350,** 216 (1991).
29. H.W. Pickering, Corrosion Sci. **23,** 1107 (1983).
30. J.S. Chen, M. Salmeron, and T.M. Devine, Corrosion Science. **34,** 2071 (1993).
31. T.B. Cassagne, W.F. Flanagan, and B.D. Lichter, Metall. Trans. A **17A,** 703 (1986).

32. N. Dimitrov, J.A. Mann, M. Vukmirovic, and K. Sieradzki, J. Electrochem. Soc. **147,** 3283 (2000).
33. R.G. Buchheit, R.P. Grant, P.F. Hlava, B. McKenzie, and G.L. Zender, J. Electrochem. Soc. **144,** 2621 (1997).
34. R.C. Newman and A. Mehta, Corrosion Sci. **28,** 1183 (1988).
35. A.D. Tomsett, H.E. Curry-Hyde, M.S. Wainwright, D.J. Young, and A.J. Bridgewater, Appl. Catal. **33,** 119 (1987).
36. A.J. Smith, T. Tran, and M.S. Wainwright, J. Appl. Electrochem. **29,** 1085 (1999).
37. A.D. Tomsett, D.J. Young, M.R. Stammbach, and M.S. Wainwright, J. Mater. Sci. **25,** 4106 (1990).
38. M.C. Simmonds, H. Kheyrandish, J.S. Colligon, M.L. Hitchman, N. Cade, and J. Iredale, Corrosion Sci. **40,** 43 (1998).
39. H.W. Pickering and Y.S. Kim, Corrosion Sci. **22,** 621 (1982).
40. K. Sieradzki and R.C. Newman, J. Phys. Chem. Solids **48,** 1101 (1987).
41. R.P. Tischer and H. Gerischer, Zeitschrift fur Elektrochemie Berichte Der Bunsengesellschaft fur Physikalische Chemie (in German) **62,** 50 (1958).
42. D.V. Pugh, A. Dursun, and S.G. Corcoran (unpublished).
43. M. Agamalian, G.D. Wignall, and R. Triolo, J. Appl. Crystallogr. **30,** 345 (1997).
44. S.G. Corcoran (unpublished, 2002).
45. M. Teubner and R. Strey, AIP **5,** 3195 (1987).
46. N.F. Berk, PRA **44,** 5069 (1991).
47. N.F. Berk, PRL **58,** 2718 (1987).
48. S.H. Chen, S.L. Chang, and R. Strey, Prog. Colloid Polym. Sci. **81,** 30 (1990).
49. S-H. Chen and S-L. Chang, J. Appl. Crystall. **24,** 721 (1991).
50. J.W. Cahn, J. Chem. Phys. **42,** 93 (1965).